PHYSICAL REVIEW C **75**, 031001(R) (2007)

Differential cross section for neutron-proton bremsstrahlung

Y. Safkan,[*] T. Akdogan,[†] W. A. Franklin, J. L. Matthews, W. M. Schmitt,[‡] and V. V. Zelevinsky[§]
Department of Physics and Laboratory for Nuclear Science, Massachusetts Institute of Technology, Cambridge, Massachusetts 02139, USA

P. A. M. Gram,[‖] T. N. Taddeucci, and S. A. Wender
Los Alamos National Laboratory, Los Alamos, New Mexico 87545, USA

S. F. Pate
Department of Physics, New Mexico State University, Las Cruces, New Mexico 88003, USA
(Received 3 May 2005; revised manuscript received 28 July 2006; published 14 March 2007)

The neutron-proton bremsstrahlung process ($np \rightarrow np\gamma$) is known to be sensitive to meson exchange currents in the nucleon-nucleon interaction. The triply differential cross section for this reaction has been measured for the first time at the Los Alamos Neutron Science Center, using an intense, pulsed beam of up to 700-MeV neutrons to bombard a liquid hydrogen target. Scattered neutrons were observed at six angles between 12° and 32°, and the recoil protons were observed in coincidence at 12°, 20°, and 28° on the opposite side of the beam. Measurement of the neutron and proton energies at known angles allows full kinematic reconstruction of each event. The data are compared with predictions of two theoretical calculations, based on relativistic soft-photon and nonrelativistic potential models.

DOI: 10.1103/PhysRevC.75.031001 PACS number(s): 13.75.Cs, 25.10.+s, 25.40.Fq

A quantitative description of the nucleon-nucleon interaction is one of the primary goals of nuclear physics. Elastic proton-proton and neutron-proton scattering have been studied in detail. There is long-standing theoretical interest in nucleon-nucleon bremsstrahlung ($NN \rightarrow NN\gamma$) as the simplest inelastic process in nucleon-nucleon scattering. The final state in this reaction contains only one additional particle, which interacts only electromagnetically. Bremsstrahlung probes the nucleon-nucleon interaction in a kinematic regime intermediate between elastic scattering (angle between scattered nucleons $\theta_{NN} \simeq 90°$; $E_\gamma = 0$) and neutron-proton radiative capture ($\theta_{NN} = 0$; $E_\gamma =$ maximum). NN bremsstrahlung necessarily involves off-shell amplitudes in the nucleon-nucleon potential, although it is now generally accepted that these are not directly measurable [1].

The lowest-order Feynman diagrams for NN bremsstrahlung are shown in Fig. 1: (a) the "external" diagram, in which the photon is emitted by one of the nucleons[1]; (b) the "internal" diagram in which the photon is emitted during the NN interaction; and (c) the rescattering diagram. The two NN bremsstrahlung reactions that are accessible to experimental study are proton-proton bremsstrahlung ($pp\gamma$) and neutron-proton bremsstrahlung ($np\gamma$). The physics of $np\gamma$ differs from that of $pp\gamma$. Because the neutron and proton can interact via the exchange of a charged meson, the internal diagram contributes in first order. Moreover, in $np\gamma$ electric dipole ($E1$) radiation is allowed, whereas in $pp\gamma$ the lowest allowed multipolarities are $E2$ and $M1$. As a consequence, $pp\gamma$ cross sections are approximately an order of magnitude smaller than $np\gamma$ cross sections. Nonetheless, many fewer experiments on $np\gamma$ than on $pp\gamma$ have been attempted, owing to the difficulty of producing intense neutron beams and of detecting at least one uncharged particle.

Prior to this work, no kinematically complete measurements of $np\gamma$ cross sections had been performed. A few doubly differential cross section measurements, with large statistical and systematic uncertainties [2,3] and inclusive photon spectrum measurements [4,5] have been reported. In the recent experiment of Volkerts *et al.* [6], proton-neutron bremsstrahlung cross sections at incident energy 190 MeV were obtained from measurements on the quasi-free channel in proton-deuteron bremsstrahlung ($pd \rightarrow ppn\gamma$). Events were kinematically selected so that the second proton is likely to be a spectator. Although these data have excellent statistical precision, they cover a somewhat smaller range in outgoing nucleon angles than in the present work and are limited to large photon angles. Moreover, the results are subject to uncertainties arising from identifying the quasifree process and extracting a free pn bremsstrahlung cross section from the quasifree cross section in a bound system (the deuteron).

Calculations of $np\gamma$ cross sections by Brown and Franklin [7] and by Herrmann, Speth, and Nakayama [8] based on nonrelativistic potential models have demonstrated the importance of the internal or meson-exchange contribution, which is seen to increase the magnitude of the cross section by as much as a factor of 2 and to significantly alter the shape of the photon angular distribution for relatively small nucleon emission angles. Similar effects are also found in the recent

[*]Present address: Overteam Technologies, Istanbul, Turkey.
[†]Present address: Physics Department, Bogazici University, Istanbul, Turkey.
[‡]Present address: The Charles Stark Draper Laboratory, Inc., Cambridge, MA 02139.
[§]Present address: 19 Winchester St., Brookline, MA 02446.
[‖]Present address: 82-1021 Kaimalu Place, Captain Cook, HI 96704.
[1]The photon may be emitted either before or after (as shown) the NN interaction and by either nucleon if both are charged.

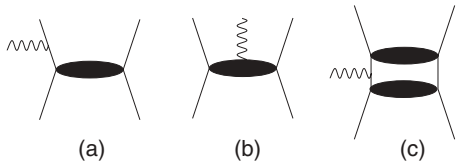

FIG. 1. Feynman diagrams for NN bremsstrahlung: (a) external process, (b) internal process, (c) rescattering process.

relativistic soft-photon analysis of NN bremsstrahlung by Timmermans *et al.* [9]. The previously measured [2,3] doubly differential $np\gamma$ cross sections $d^2\sigma/d\Omega_n d\Omega_p$ tend to exceed the calculations [7,8] for larger values of θ_n and θ_p. However, because no photon angular distributions were extracted from these data, no stringent tests of theory could be made.

In this article we report on the first measurement [10] of the triply differential $np\gamma$ cross section—the photon angular distribution for specific neutron and proton angles—in the incident neutron energy region between 175 and 275 MeV. At the LANSCE-WNR facility at the Los Alamos National Laboratory, a pulsed neutron beam is produced by an 800-MeV proton beam incident on a 7.5-cm-long water-cooled tungsten spallation target. The proton pulse width (<0.5 ns) and pulse spacing (1.8 μs) allow time-of-flight techniques to be used. The beam was defined by horizontal and vertical copper shutters (3.8 × 3.8 cm opening × 40 cm long), passed through a sweep magnet to eliminate charged particles and then collimated by 9 m of iron to create a well-defined 2.5-cm diameter beam spot at the $np\gamma$ target. The neutron flight path length from the spallation source to the target is 18 m. Before reaching the target, the neutron beam traversed a ^{238}U fission ionization chamber [11], in which the yield of fission fragments was used to determine the incident neutron flux.

The liquid hydrogen target consisted of a vertical, thin-walled (50 μm Aramica) cylindrical flask with a diameter of 7.6 cm, placed inside a 32-cm diameter vacuum chamber. The target was operated at a temperature of 15K and a pressure of 96.5 kPa, yielding an areal density of 0.32 atoms/b.

Outgoing protons and neutrons were observed in two coplanar arrays of detectors, one in the horizontal plane and one inclined at ∼25° to the horizontal. Protons were detected using pure CsI crystals, placed at polar angles of 12°, 20°, and 28° in each array. Each detector subtended a solid angle of about 8.5 msr. Thin plastic ΔE detectors attached to the front faces of the crystals provided particle identification information. Neutron detectors, which were liquid or plastic scintillators subtending solid angles of about 3 msr, were placed at polar angles of 12°, 16°, 20°, 24°, 28°, and 32° in each array on the opposite side of the beam. The front faces of the neutron detectors were covered by thin plastic "veto" detectors to reject charged-particle events. All detector gains and timing stability were monitored continuously using light pulses from a nitrogen laser transmitted through optical fibers to each photomultiplier tube [12,13].

The proton energies are determined by pulse height information from the CsI detectors. The pulse height *vs.* kinetic energy calibration is performed using elastic np scattering, which dominates the events recorded when the data acquisition system is triggered by "proton singles." The elastic protons are thus easily identified.

The arrival times of the scattered neutrons and recoil protons at their respective detectors are measured relative to the arrival time of the proton pulse at the spallation source. An independent determination of the proton kinetic energy, based on the pulse height measurement, makes it possible to determine the times of flight of the incident neutrons from the spallation source to the hydrogen target and of the scattered neutrons from the target to the detectors.

Because the maximum opening angle between the neutron and proton detectors is 60°, all real np coincidence events must result from inelastic scattering. Below the π-production threshold, the only inelastic process is $np \rightarrow np\gamma$. Candidate bremsstrahlung events are those comprising a charged particle (a count in both detectors of a given ΔE-CsI pair) in coincidence with a neutral particle (a count in a neutron detector but not in its corresponding veto). The data are further reduced using proton identification (from the E *vs.* ΔE information) and neutron identification (from the maximum possible recoil proton pulse height in the neutron detector for a neutron arriving with a given time of flight) criteria.

The experimental data must be corrected for two types of background, that from the empty target flask and that from random coincidences. Real np coincidences can result from quasifree (n, np) processes in the ^{12}C and ^{16}O nuclei in the target flask and scattering chamber windows. Although the combined thickness of these windows is a factor of ∼100 less than that of the liquid hydrogen, the (n, np) cross section is a factor of ∼100 larger than that for $np\gamma$, making this background comparable to the foreground. Moreover, it cannot be measured simply by emptying the target: the presence of the liquid hydrogen in the full target produces significant proton energy loss that is absent when the target is empty. This effect must be simulated and corrected for in the subtraction of the empty-target data.

Compared with the real coincidence rate from $np\gamma$, the random coincidence rate is large for three reasons: the large np elastic scattering cross section (about three orders of magnitude greater than that for bremsstrahlung), the large ambient neutron background, and the (necessarily) low duty factor of the incident pulsed neutron beam. This background was measured by combining uncorrelated "singles" events from the proton and neutron detectors. The result was then normalized using the count rate in a kinematically impossible region and subtracted from the full-target data.

The efficiencies of the neutron detectors, which varied between 7 and 12% over the energy range of the experiment, were measured with an overall uncertainty of ∼7% by placing the detectors in elastic np scattering geometry. Although the proton detectors are essentially 100% efficient for charged particles, strong interactions in the CsI will cause some protons to be misidentified. The resulting inefficiency was determined using the proton singles events, which are dominated by np elastic scattering.

For a given incident neutron energy, knowledge of the detector angles and measurement of the scattered neutron and recoil proton energies uniquely determine the energy and emission angle of the undetected photon. The solid curve in

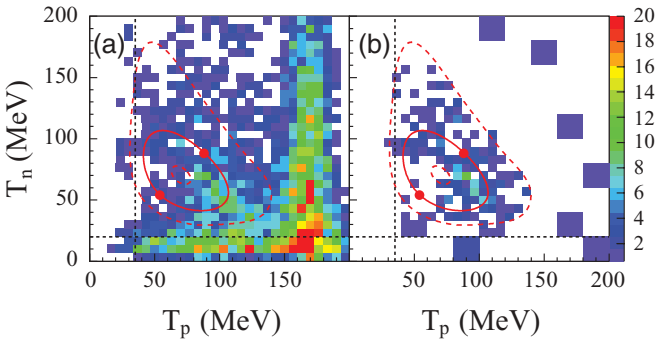

FIG. 2. (Color) (a) Full-target data for mean incident neutron energy $T_{\rm inc} = 225$ MeV and $\theta_n = \theta_p = 28^\circ$, plotted as a function of scattered neutron and proton kinetic energies. (b) Data after subtraction of empty-target and random-coincidence background. The solid curve is the kinematic locus for $T_{\rm inc} = 225$ MeV along which np bremsstrahlung events should fall. The solid circles indicate emitted photon angles of 0° and 180° at low and high nucleon energies, respectively. The lower (upper) portion of the curve between 0° and 180° corresponds to photons emitted on the neutron (proton) side of the beam. The vertical (horizontal) short-dashed line represents the proton (neutron) detection threshold. The long-dashed curves illustrate a kinematic cut as described in the text.

Figs. 2(a) and 2(b) is the kinematic locus on which $np\gamma$ events will fall, for an incident energy of 225 MeV and $\theta_n = \theta_p = 28^\circ$. In Fig. 2(a) data from the full target are plotted as a function of T_n and T_p. For this presentation, data in the incident energy range 175–275 MeV are included, with the measured neutron and proton momenta scaled to correspond to $T_{\rm inc} = 225$ MeV. Figure 2(b) shows the same data after subtraction of the empty-target and random-coincidence backgrounds. The latter subtraction removes the large concentration of events seen in Fig. 2(a) at $T_p \approx 170$ MeV; this is the recoil proton energy in np elastic scattering at 28°. To obtain the $np\gamma$ cross section, kinematic cuts based on a Monte-Carlo analysis of the finite-size effects and resolution of the experiment were applied to the data. The long-dashed curves represent the kinematic cut for $T_{\rm inc} = 225$ MeV. In the analysis of the data, the cuts used are a function of the outgoing nucleon energies and angles *and* the incident beam energy. The area enclosed by the two long-dashed curves becomes a toroidal volume, and all the events that lie in this volume are accepted.

In principle, the $np\gamma$ cross section could be obtained as a function of incident neutron energy from a lower limit determined by proton energy losses and particle detection thresholds up to the maximum energy neutrons ($\sim$700 MeV) produced by the spallation source. In practice, the highest incident neutron energy for which we could measure the $np\gamma$ cross section at all angles was $\sim$300 MeV, due to the onset of the $np \rightarrow np\pi^0$ process, whose cross section is much larger than that for $np\gamma$. Above the π^0-production threshold the experiment did not have adequate resolution in missing mass to distinguish the γ and π^0 final states.

Theoretical calculations by Brown [14] and by Liou [15] for incident neutron energies 175 and 275 MeV showed the energy dependence of the $np\gamma$ cross section to be much smaller than the experimental uncertainties at all observed nucleon angles. Accordingly, in presenting the results we have summed the cross sections obtained over this incident energy range. For each pair of neutron and proton angles, a photon angular distribution was constructed. The data from each of the two coplanar arrays, after checking for consistency, were summed for each angle pair.

Data were obtained during approximately six months of accelerator running. The integrated beam flux in the 175–275 MeV energy range incident on the full and empty hydrogen target was 6×10^{12} and 4×10^{12} neutrons, respectively.

As a representative sample of the data, triply differential cross sections for six of the 18 neutron-proton angle pairs observed are shown in Fig. 3. The gaps in the angular distributions for negative (positive) angles are a consequence of the corresponding neutron (proton) kinetic energies lying below the detection thresholds. These data and those at the other observed angle pairs with $\theta_{n,p} \geqslant 20^\circ$ clearly establish an asymmetry in the photon angular distribution: the cross section is larger for photons emitted on the neutron side than for photons emitted on the proton side of the beam. As is shown explicitly in Refs. [7–9], such an asymmetry arises from inclusion of meson exchange currents—the "internal" diagram in Fig. 1(b).

The curves are results of the theoretical calculations of Brown and Franklin [7,14] and Timmermans *et al.* [9]. The agreement with the data is seen to be moderately good in most cases; however, there is a tendency for the theory to underpredict the measurement. This is particularly evident in the "neutron-side" region of the angular distributions for $\theta_p = \theta_n = 20^\circ$ [Fig. 3(c)] and $\theta_p = \theta_n = 28^\circ$ [Fig. 3(e)].

The finite sizes of the proton and neutron detectors correspond to an azimuthal (out-of-plane) angular range of about $\pm 4^\circ$, which translates into a possible out-of-plane angle for the undetected photon of as much as $\pm 20^\circ$. To investigate this effect, we have performed a Monte Carlo average of the out-of-plane cross sections recently calculated by Brown [14,17] and by Timmermans [9,18] over the detector acceptances. The results are indicated by the blue and red shaded bands in Fig. 3(e). The average effect on the cross section of noncoplanarity of the detected nucleons is seen to be small.

A comparison of our results with those of Volkerts *et al.* [6] is possible at only one set of kinematics. In Fig. 3(a) the present results at $\theta_n = \theta_p = 12^\circ$ are shown along with the previous results at $\theta_n = 13.5^\circ$, $\theta_p = 12^\circ$, and incident energy 190 MeV. The agreement between the two measurements is satisfactory within the experimental uncertainties, and tends to support the validity of the renormalization factor of 0.4, which, although not understood, was applied to the previous data [6].

In summary, a measurement of the triply differential cross section for neutron-proton bremsstrahlung has been performed over a broad kinematic range, utilizing a pulsed neutron beam incident on a liquid hydrogen target with coincident detection of scattered neutrons and recoil protons. The asymmetric shapes of the measured photon angular distributions are consistent with those calculated with the exchange current contribution included, a theoretical prediction that had not been

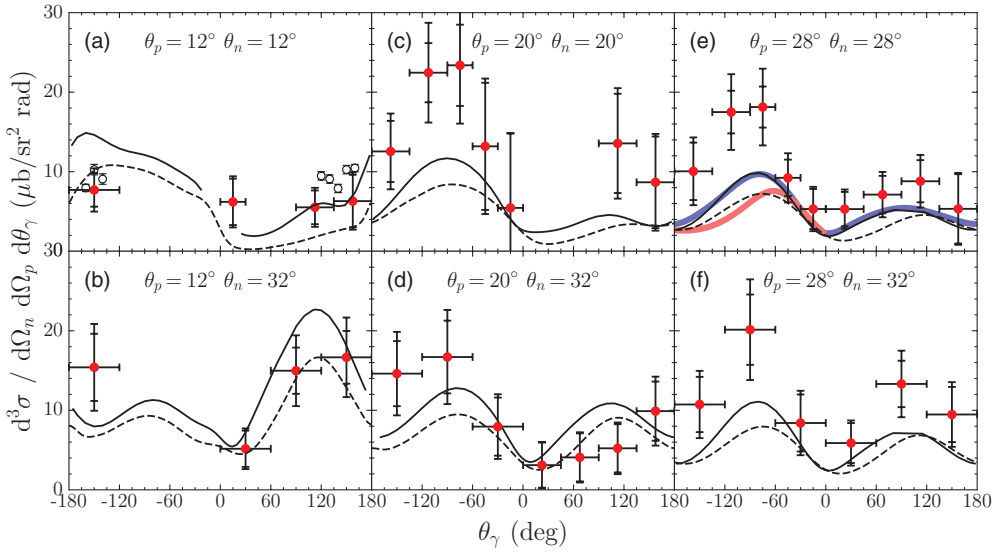

FIG. 3. (Color) Photon angular distributions in np bremsstrahlung for (a) $\theta_p = \theta_n = 12^\circ$; (b) $\theta_p = 12^\circ, \theta_n = 32^\circ$; (c) $\theta_p = \theta_n = 20^\circ$; (d) $\theta_p = 20^\circ, \theta_n = 32^\circ$; (e) $\theta_p = \theta_n = 28^\circ$; (f) $\theta_p = 28^\circ, \theta_n = 32^\circ$. Negative (positive) angles correspond to photons emitted on the neutron (proton) side of the beam. The data (solid circles) have been summed over the incident neutron energy range 175–275 MeV; the inner error bars are the statistical uncertainties; the outer error bars include systematic uncertainties [16]. The curves are the theoretical predictions of Brown [7,14] (solid curves) and Timmermans *et al.* [9] (dashed curves). The blue and red shaded bands represent an average over the detector acceptances of the predictions of Brown [17] and Timmermans *et al.* [18], respectively, with out-of-plane contributions included. The open circles in (a) are quasifree pn bremstrahlung cross sections at $\theta_n = 13.5^\circ, \theta_p = 12^\circ$, and incident energy 190 MeV from the pd bremsstrahlung experiment of Volkerts *et al.* [6]. The statistical uncertainties are comparable to the size of the symbols.

tested experimentally. The present results confirm the excess of measurement over theory suggested by previous doubly differential cross section data, indicating that deficiencies remain in the theoretical models. The present data, albeit with limited statistical precision, provide a challenge to modern calculations of this fundamental process in the nucleon-nucleon interaction.

We acknowledge J. da Graça, M. A. Greene, and L. W. Kwok for their assistance in setting up the experiment and acquiring the data. We thank V. R. Brown and B. F. Gibson for valuable guidance on theoretical issues and for making available their unpublished calculations. This work was supported in part by funds provided by the U.S. Department of Energy.

[1] H. W. Fearing, Phys. Rev. Lett. **81**, 758 (1998).
[2] F. P. Brady, J. C. Young, and C. Badrinathan, Phys. Rev. Lett. **20**, 750 (1968); F. P. Brady and J. C. Young, Phys. Rev. C **2**, 1579 (1970); **7**, 1707 (1973).
[3] J. A. Edgington *et al.*, Nucl. Phys. **A218**, 151 (1974).
[4] F. Malek *et al.*, Phys. Lett. **B266**, 255 (1991).
[5] D. R. Mayo, Ph.D. dissertation, University of California, Davis (1997).
[6] M. Volkerts *et al.*, Phys. Rev. Lett. **92**, 202301 (2004).
[7] V. R. Brown and J. Franklin, Phys. Rev. C **8**, 1706 (1973).
[8] V. Herrmann, J. Speth, and K. Nakayama, Phys. Rev. C **43**, 394 (1991).
[9] R. G. E. Timmermans, T. D. Penninga, B. F. Gibson, and M. K. Liou, Phys. Rev. C **73**, 034006 (2006); M. K. Liou (private communication, 2002).
[10] Y. Safkan, Ph.D. thesis, Massachusetts Institute of Technology, 2001.
[11] S. A. Wender *et al.*, Nucl. Instrum. Methods A **336**, 226 (1993).
[12] B. T. Marshall, S. B. thesis, Massachusetts Institute of Technology, 1993.
[13] V. V. Zelevinsky, S. B. thesis, Massachusetts Institute of Technology, 1994.
[14] V. R. Brown (private communication, 2004).
[15] B. F. Gibson (private communication).
[16] The total systematic uncertainty is approximately 19%, with the major contributions due to uncertainties in the neutron beam flux determination, the neutron detector efficiencies, and the geometrical acceptances of the detectors.
[17] V. R. Brown (private communication, 2006).
[18] R. Timmermans (private communication, 2006).